Time-Domain Characterization of Nematic Liquid Crystals Using Additive Manufacturing Microstrip Lines

Pablo Mateos-Ruiz⬭, Mario Pérez-Escribano⬭, Alberto Hernández-Escobar⬭,
Elena Abdo-Sánchez⬭, *Member, IEEE*, Enrique Márquez-Segura⬭, *Senior Member, IEEE*,
Teresa M. Martín-Guerrero⬭, *Senior Member, IEEE*, and Carlos Camacho-Peñalosa⬭, *Life Senior Member, IEEE*

Abstract— This article presents a method for effectively characterizing the dielectric permittivity of nematic liquid crystals (LCs) across a broad frequency range. These materials show significant potential for reconfigurable devices operating in microwave and millimeter-wave frequencies. To achieve this goal, an additive manufacturing technique is used to create a microstrip line that can be filled with liquid that acts as its substrate. The LC is then biased to modulate its permittivity. After manufacturing, a time-gating approach is used to extract the permittivity, eliminating the need for in-fixture calibration, such as thru–reflect–line (TRL). Finally, the approach is validated through simulations and experimental results, which closely align with those reported using other methods in the bibliography.

Index Terms— Broadband measurements, liquid crystals (LCs), permittivity characterization, reconfigurability, time gating.

I. INTRODUCTION

THE rapid development of wireless communication services requires reconfiguring the radiation patterns of antenna systems efficiently and cost-effectively to adapt themselves to the changing environment. Some examples of applications of tunable antennas are 5G/6G services or automotive radars. Traditionally, fixed-frequency beam steering has been achieved either mechanically, which results in bulky structures, or by implementing phased arrays, which lead to complex and expensive feeding networks. An alternative technology to reconfigurable components, such as varactors or micromechanical actuators, is nematic liquid crystals (LCs) [1]. These tunable materials are potential candidates for reconfigurable antennas [2], especially at high frequencies for which mechanical actuators and integrated devices suffer high transmission losses. In addition, tunable materials have the main advantage of reconfiguring the whole structure at once for modern directive planar antennas, such as reflect arrays [3], [4], leaky wave [5], or metasurface-based antennas [6]. They have also been used for other reconfigurable devices, such as filters [7] or phase shifters [8].

In their nematic phase, LCs are anisotropic materials with tunable electric permittivity through a biasing voltage [9]. In [10], a dispersion analysis of anisotropic periodic structures applied to LCs was performed. Although LCs for optical applications have been studied extensively, their use is not so extended at microwave frequencies. The broadband characterization of its effective dielectric constant is required to enable the design of reconfigurable antennas using such a technology. In general, dielectric and transmission line characterization methods have been divided into two groups: resonant and broadband. Resonant characterization methods have been presented in the literature, using multilayer structures based on microstrip transmission lines [11] or planar patch resonators [12] among others, but they are inherently narrowband. Another multilayer structure for the extraction of permittivity as a function of the bias voltage is presented in [13]. In [14], a broadband characterization method was proposed, which needs thru and line standards to carry out the calibration and, thus, requires fabricating and measuring additional structures.

There has been research on the characterization of LCs in the time domain for many years [15], [16]. Time-gating techniques have been traditionally used to avoid undesired effects, such as noise or reflections. In devices whose different section responses are not physically separable, the undesired section contributions can still be mostly removed
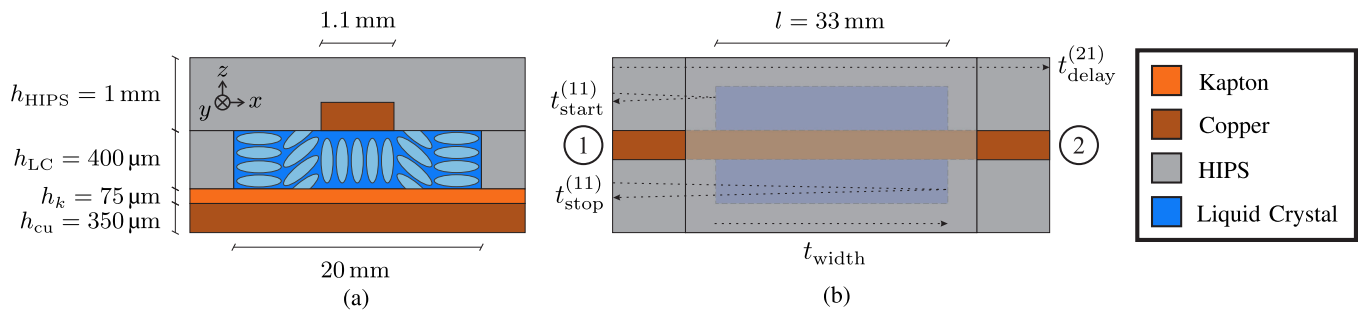
Fig. 1. Not-to-scale diagram of (a) stack-up with the LC molecules polarized and (b) top view of the proposed covered microstrip line.

in the time domain (see [17]), enabling dielectric materials characterization [18]. This contribution proposes a time-gating technique to characterize the relative permittivity of LCs inside microstrip lines fabricated using additive manufacturing. This approach allows the fabrication and measurement of a single prototype while enabling broadband characterization. The main advantage is that it does not require any in-fixture calibration of the analyzer [19], [20] or the use of more than one transmission line when using differential length characterization techniques [21], [22], which considerably facilitates its application due to the difficulty of manufacturing this type of structure.

This article is organized as follows. Section II describes the stack-up of the proposed structure. Section III illustrates the proposed method based on time gating to extract the dielectric permittivity of the LC. Section IV shows the validation through simulation and experimental results. Finally, the conclusions are drawn in Section V.

II. STRUCTURE DESCRIPTION

The proposed microstrip transmission line stack-up is shown in Fig. 1(a). As seen, it consists of four layers. The first one from the bottom is made of copper and plays the role of ground plane. The second layer is a thin polyimide (kapton) sheet to ensure the correct LC molecules orientation at rest [1]. The third one is the pool where the LC is contained, whereas the pool edges are made of high-impact polystyrene (HIPS) using additive manufacturing. Fig. 1(b) shows a top view of the structure described. In the top layer is a strip milled from a 350-μm-thick copper sheet and an overlay of HIPS with a groove in which the strip fits and stays correctly suspended above the LC pool. In this layer, two perforations allow the liquid crystal pool to be filled using a syringe. All junctions between layers are performed using screws located outside the pool and nonconductive epoxy to prevent fluid leakages. Fig. 1 details the structure's main dimensions.

Regarding HIPS, it was proposed for microwave applications and characterized in [23]. It is a material for fused filament fabrication with excellent electromagnetic properties due to its low loss tangent and relative permittivity, close to 2.45. In addition, HIPS is durable and possesses good impact resistance together with the fact that remains stable when exposed to moisture. For the proposed experiment, it was printed out using the Ultimaker 3 printer, setting the infill to
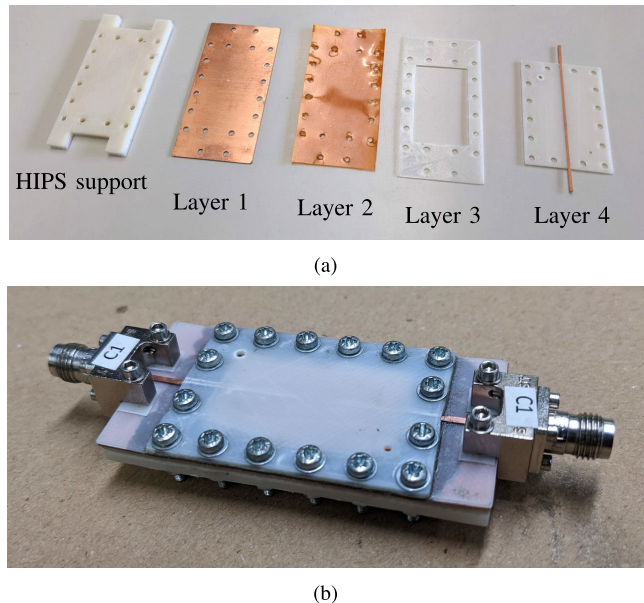

Fig. 2. Fabricated prototype (a) as a side-by-side view of its layers and (b) fully assembled and sealed.

100%. The extrusion and bed temperatures were established to 240 °C and 90 °C, respectively, and the layer height was set to 60 μm. The HIPS layers (including structural support), along with the rest of them used in the structure, are shown side by side in Fig. 2(a) and the assembled and sealed prototype in Fig. 2(b).

III. CHARACTERIZATION METHOD

A. Time Gating

The time-domain processing from frequency-domain measurements is used to remove the undesired contribution from the sections of the transitions between the ports and the pool [see Fig. 1(b)], thus moving the reference planes to the pool outer interfaces. First, the measured S-parameters are resampled to present 2^n frequency points evenly spaced along the whole bandwidth, starting from dc. As the original measurements from a vector network analyzer will probably not include dc, a sensible assumption is to consider it a short circuit. So, an inverse fast Fourier transform (IFFT) is adequately applied to every S-parameter to obtain their time-domain responses. These are the convolution of the impulse responses with a sinc function due to the measured frequency

response truncating the actual band-unlimited one. Another type of window (Hamming, Blackman, and so on) can be applied before the IFFT to reduce the impulse response widening and, thus, improve its visualization. Furthermore, applying frequency-domain zero padding in the IFFT is recommended to increase time resolution. Then, if the zero-padding order n_z represents the factor by which the number of frequency points is increased, the achieved time resolution will be $dt = 1/(2n_z f_{max})$, with f_{max} being the maximum measured frequency.

The time interval related to the LC section (when does it start, $t_{start}^{(11)}$, and end, $t_{stop}^{(11)}$) can be derived from previous knowledge of the structure dimensions and the widened impulse response of the S_{11}. This time response will be composed of several widened deltas, among which the $t_{start}^{(11)}$ timestamp will correspond with the peak of one of the most relevant ones, and for which a fine time resolution is needed for its proper identification. In addition, as the structure shown in Fig. 1(b) is symmetric and its delay $t_{delay}^{(21)}$ can be obtained as the main peak timestamp in the S_{21} time response, $t_{stop}^{(11)}$ directly arises from $t_{start}^{(11)}$, once derived, as follows:

$$t_{stop}^{(11)} = 2\, t_{delay}^{(21)} - t_{start}^{(11)}. \tag{1}$$

The time-gate width can then be calculated as follows:

$$t_{width} = \left(t_{stop}^{(11)} - t_{start}^{(11)}\right)/2 \tag{2}$$

which is divided by two to account for the round trips in the reflection signals, as shown in Fig. 1(b).

This way, the time-gating timestamps for the rest of the S-parameters can be geometrically derived from the port-1 timestamps. Transmission parameters time responses will consist of a main pulse (whose peak's timestamp determines the signal delay between both ports) followed by the contributions of several internal reflections. Using the t_{width} value also for these parameters, the timestamps for the transmission from port 1 to port 2, for example, would be

$$\begin{aligned} t_{start}^{(21)} &= t_{delay}^{(21)} - t_{width}/2 \\ t_{stop}^{(21)} &= t_{delay}^{(21)} + t_{width}/2 \end{aligned} \tag{3}$$

thus applying the time gate around the main pulse arrival. For reflection parameters, the corresponding timestamps can be geometrically derived from Fig. 1(b), provided that the time delay between port 1 and the port of interest is already known. For example, port-2 reflection timestamps would be calculated as follows:

$$\begin{aligned} t_{start}^{(22)} &= 2\, t_{delay}^{(21)} - t_{stop}^{(11)} \\ t_{stop}^{(22)} &= 2\, t_{delay}^{(21)} - t_{start}^{(11)}. \end{aligned} \tag{4}$$

Following the approach from [24], a high-order Butterworth filter window is used as the time gate to prevent amplitude distortion within the interval of interest (from t_{start} to t_{stop}) while significantly attenuating the rest of the response without introducing abrupt changes. The corresponding time window is multiplied by each impulse response, and the result is shifted toward the time origin to remove the undesired sections'

contribution to the equivalent transmission line length. The time shift will depend on the specific parameter

$$\begin{aligned} t_{shift}^{(ii)} &= t_{start}^{(ii)} \\ t_{shift}^{(ji)} &= t_{delay}^{(ji)} - t_{width}. \end{aligned} \tag{5}$$

Finally, the impulse responses are transformed back to the frequency domain by applying a fast Fourier transform (FFT), reverting zero padding and dividing by the used frequency window to remove the amplitude distortion, if needed. Thus, an approximation of the LC section's S-parameters is obtained.

B. Permittivity Extraction

Considering that the processed S-parameters have a good impedance matching and represent a transmission line, then its effective permittivity can be estimated from the transmission parameter

$$S_{21} = e^{-jkl} = e^{-\alpha l} e^{-j\beta l} = e^{-j\frac{2\pi f}{c_0}\sqrt{\varepsilon_{eff}}l} \tag{6}$$

where l is the pool length [Fig. 1(b)]. To extract ε_{eff} from the complex exponential without facing problems related to the phase wrapping and phase reference, its value is reconstructed from both the magnitude and the unwrapped phase of S_{21} as follows:

$$\sqrt{\varepsilon_{eff}} = \sqrt{\varepsilon' - j\varepsilon''} = x + jy \tag{7}$$

$$|S_{21}| = |e^{-\alpha l}| \Rightarrow y = \frac{c_0}{2\pi f l} \log|S_{21}| \tag{8}$$

$$\angle S_{21} = -\beta l \Rightarrow x + f\frac{\partial x}{\partial f} = -\frac{c_0}{2\pi l}\frac{\partial \text{unwrap}(\angle S_{21})}{\partial f} \tag{9}$$

$$\varepsilon_{eff} = (x^2 - y^2) + j(2xy). \tag{10}$$

The first-order differential equation from (9) can be numerically solved. Thus, by inserting (8) and (9) into (10), the LC-section effective relative permittivity is calculated. For this process, it is assumed that there is a linear S_{21} phase variation with frequency, which is the natural behavior in a transmission line.

However, this work aims to characterize the liquid crystal's nominal permittivity ε_r, not the whole stack of different materials. Hence, a multilayered microstrip model is considered. First, the HIPS overlay used to seal the LC container is taken into account using the model from [25], which, although not frequency-dependent, allows the direct calculation of the microstrip substrate permittivity ε_r' from ε_{eff}. In addition, the substrate comprises both LC and Kapton. The latter is well known and used in microwave applications, having a relative permittivity $\varepsilon_{r_k} = 3.5$. The equivalent single-layer permittivity of these materials can be obtained using [26]

$$\varepsilon_r' = \frac{\varepsilon_{r_k}\varepsilon_r(h_k + h_{LC})}{\varepsilon_{r_k}h_{LC} + \varepsilon_r h_k}. \tag{11}$$

This model can be used considering the liquid crystal as a lossy dielectric, since it only considers the electromagnetic properties of the material (ε_r and $\tan\delta$) and not its mechanical characteristics, which also change with the bias voltage. Knowing the layers heights [see Fig. 1(a)], the LC permittivity ε_r can be retrieved from the previously calculated substrate permittivity ε_r' through (11).

On the other hand, determining the loss tangent requires reliable information solely about the transmission magnitude of the pool section. Applying the time gate in the middle of an already brief time response induces distortion in the reflection response and results in the main transmission response peak being a composite of inseparable contributions from the entire prototype. Consequently, when time gating the transmission response around the main peak, only the contribution of secondary internal reflections occurring outside the time gate will be eliminated (thus conveniently smoothing the transmission parameter). Nevertheless, the magnitude of the gated peak remains identical to that of the original ungated response. Therefore, deriving a loss tangent from this parameter lacks physical validity, as it would encompass losses from undesired sections outside the pool, thereby distorting the actual pool-section losses.

IV. VALIDATION

In this section, both preliminary simulation tests and experiments using a manufactured prototype will be carried out using the GT7-29001 LC from Merck, which offers $\{\varepsilon_{r_\perp} = 2.46, \tan\delta_\perp = 0.0116\}$ and $\{\varepsilon_{r_\parallel} = 3.53, \tan\delta_\parallel = 0.0064\}$ at 19 GHz, according to available datasheet.

A. Simulation Test

The structure is first simulated in ANSYS HFSS to verify the proper signal processing operation with ideal and controlled data. Three cases are simulated: with the pool filled with LC in ON- and OFF-states and air used as a reference. The whole pool, entirely filled with LC, is assumed to offer the permittivity $\varepsilon_{r_\perp}$ in the electric field main direction for the OFF-state. In the ON-state, however, the LC will not be homogeneously polarized for two main reasons. First, under electric field biasing, the LC molecules orient differently along the LC height, with a behavior modeled by the differential equations governing the nematic LCs physics [27], [28]. This effect translates into average LC molecules tilt angle θ_m, concerning the OFF-state, that will be lower than 90°. Then, the LC permittivity tensor can be calculated in the chosen coordinates system and biasing field direction as follows:

$$\overline{\overline{\varepsilon_r}} = \begin{pmatrix} \varepsilon_\perp + \Delta\varepsilon_r \cos^2\theta_m & 0 & \Delta\varepsilon_r \cos\theta_m \sin\theta_m \\ 0 & \varepsilon_\perp & 0 \\ \Delta\varepsilon_r \cos\theta_m \sin\theta_m & 0 & \varepsilon_\perp + \Delta\varepsilon_r \sin^2\theta_m \end{pmatrix} \quad (12)$$

where $\Delta\varepsilon_r = \varepsilon_{r_\parallel} - \varepsilon_{r_\perp}$. Nevertheless, θ_m can be easily calculated through [2], and from which it can be concluded that for sufficiently high biasing voltages, $\theta_m \approx 90°$, allowing this effect to be neglected in simulations.

The second cause for inhomogeneity comes from the bias voltage being applied to the microstrip itself, thus only fully polarizing the LC immediately below it and partially polarizing the LC beyond the microstrip width. Hence, as the microstrip width is not much greater than the pool height, the fringing fields' contribution to the effective permittivity should be considered [3]. Thus, the ON-state is simulated by stratifying the pool media, where the LC below the line presents a permittivity tensor given by (12) with $\theta_m = 90°$,
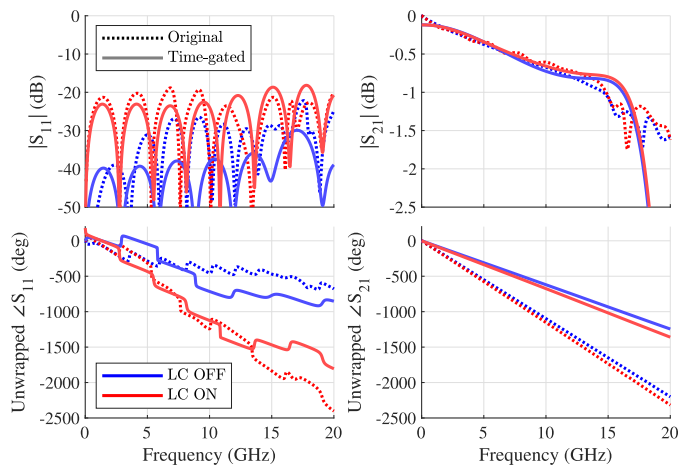

Fig. 3. Original and time-gated simulated S-parameters for the ON and OFF LC states.

the LC alongside the microstrip (with a width equal to the microstrip width on each side) has $\theta_m = 45°$, and the rest is assumed not polarized at all, just as schematically shown in Fig. 1(a). From simulations and bibliography, this scenario was chosen as a good estimation.

The S-parameters obtained from the simulations for the LC-filled pool cases are presented in Fig. 3 with dotted lines, where a good matching and a linear transmission phase variation are appreciated, as expected. These are transformed to the time domain after applying a Hamming window to improve visualization, and the resulting S_{11} and S_{21} time responses are represented in Fig. 4 with dotted lines. The first reflection peak, where the three responses begin to differ, indicates the timestamp when the pool section starts $t_{\text{start}}^{(11)} = 133$ ps (represented with a black dashed vertical line). The structure delay for each case is obtained as the timestamp of the main transmission peak. Then, as explained in Section III-A, due to the structural symmetry, the timestamps when the pool ends $t_{\text{stop}}^{(11)}$ are automatically obtained for each case (represented with vertical dashed lines colored as their corresponding response), coinciding with the reflection peaks at the exit of the pool section, which is electrically longer as the filling substrate permittivity increases.

Note that the 20-GHz simulated bandwidth would give a time resolution of $dt = 25$ ps, too coarse for the proper determination of the time-gating timestamps in such a small device. Consequently, an IFFT zero-padding order of $n_z = 50$ was used, thus giving a smaller step $dt = 0.5$ ps. From tests with the studied configuration, the steps of dt in the $t_{\text{start}}^{(11)}$ value produce variations less than ±0.02 in the obtained pool section ε_{eff}.

The time responses are time gated using the obtained timestamps, resulting in the solid lines in Fig. 4. $t_{\text{start}}^{(11)}$ becomes the new time origin for the reflection response, the transmission one is shifted following (5), and the responses are transformed back to the frequency domain, resulting in the time-gated S-parameters represented in Fig. 3 with solid lines, from which the processing described in Section III-B is carried out. The obtained permittivities are shown in Fig. 5, from the complete DUT to the extracted pool-media ones. In addition,
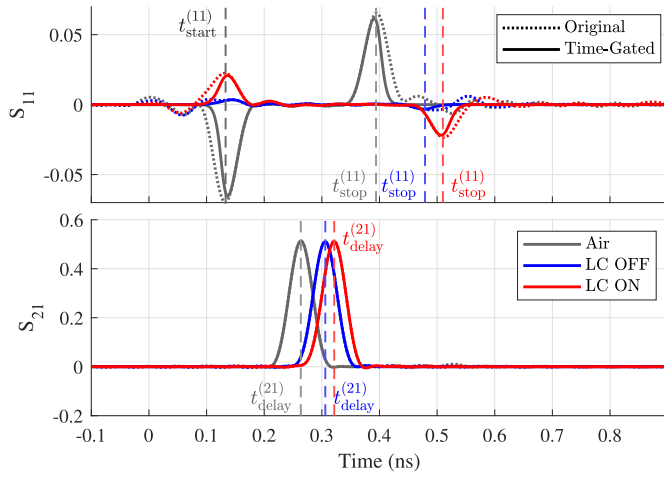
Fig. 4. Widened impulse responses of the simulated S_{11} (up) and S_{21} (down) before and after the time gating, and with their timestamps.
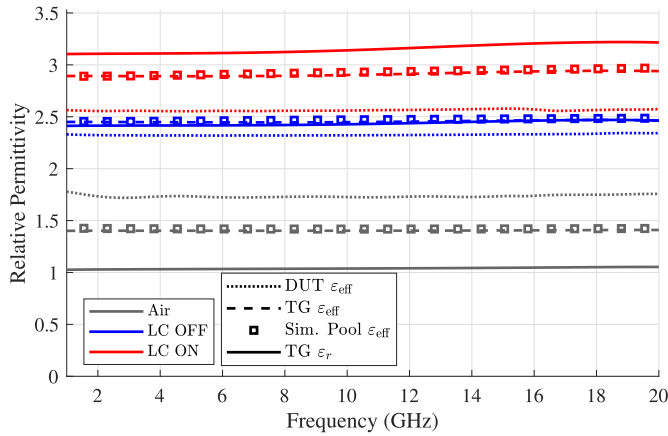

Fig. 5. Relative permittivities obtained from the processed simulations for different pool substrate scenarios.

Fig. 6. Comparison of simulation extracted ε_r for different applied frequency windows.

the time window itself mainly distorts the lowest frequencies, so the results are always shown from 1 GHz onward, except in Fig. 6 for illustrating the explained artifacts. This should not be an issue for reconfigurable devices designed for microwave frequencies.

B. Experimental Results

The fabricated prototype is shown in Fig. 2(b). Southwest 2.4-mm end launch connectors are used, whose contribution will also be removed through time gating. Port 1 of the prototype is connected to a bias T, where the 1-kHz sinusoidal bias signal is input, and port 2 is connected to a dc block. The measurements are carried out with a Keysight PNA-X N5247A network analyzer configured with a frequency sweep of 6401 points from 10 MHz to 20 GHz. The bandwidth of the intermediate frequency (IF) bandpass filter is set at 10 kHz, whereas the port power is −5 dBm.

As in Section IV-A, the S-parameters are measured for the same three pool-media cases (air, LC OFF, and LC ON). In addition, for the LC ON-state, two biasing voltages are tested, 20 V_{pp} and 100 V_{pp}, and the measurements are presented in Fig. 7 as dotted lines, which are saved upon the stabilization of the S_{21} phase. Worse matching and greater losses concerning simulations are appreciated, which can be attributed to manufacturing imperfections, the applied epoxy, and the connectors. The time responses obtained from applying the same processing as in Section IV-A are shown in Fig. 8. In this case, it may not be so evident which $t_{start}^{(11)}$ value should be selected, as the responses are expectably not as clean as in simulations. Thus, the air-filled pool case is advantageous to undergo a final calibration, ensuring its extracted relative permittivity is consistently close to 1 along the bandwidth. This is achieved by choosing $t_{start}^{(11)} = 235$ ps, higher than in simulations due to the connectors contribution.

The time-gated S-parameters are shown as solid lines in Fig. 7. Note that although a quantitative assessment of the LC $\tan \delta$ cannot be carried out, the material is qualitatively behaving as expected, offering lower losses as it is increasingly polarized. Fig. 9 presents the permittivity values extracted from these parameters. It is observed how the time gating and then the multilayered model effectively transform the permittivity values from those of the whole structure to the pool media ones. The results, although not as ideal, are

the effective permittivity of the pool section alone has also been simulated, and it is in excellent agreement with the one obtained from the time-gated parameters, thus validating the time-gating approach.

The reference air-filled case gives a ε_r close to 1, thus confirming the proper selection of the time-gating timestamps. It can be noted that the OFF-state LC ε_r is practically equal to $\varepsilon_{r_\perp}$, while for the ON-state, the LC permittivity that the microstrip "perceives" is lower than $\varepsilon_{r_\parallel}$ (which is the plot ordinate higher limit) due to the LC anisotropy and the stratified media configuration, which prevents the full polarization of the whole LC filling the pool. These results will serve as a reference for the real experiments.

The choice of the particular frequency window applied before the IFFT must take into account that, although higher time-domain sidelobe suppression could facilitate the main widened deltas recognition, they also significantly suppress higher frequencies, which degrades the permittivity extraction accuracy in that range. This effect is shown in Fig. 6 for different applied frequency windows, from where it is clear that the majority of the bandwidth remains unaffected. After correct timestamp determination, the frequency window offering less distortion in the band edge should be used. Moreover,
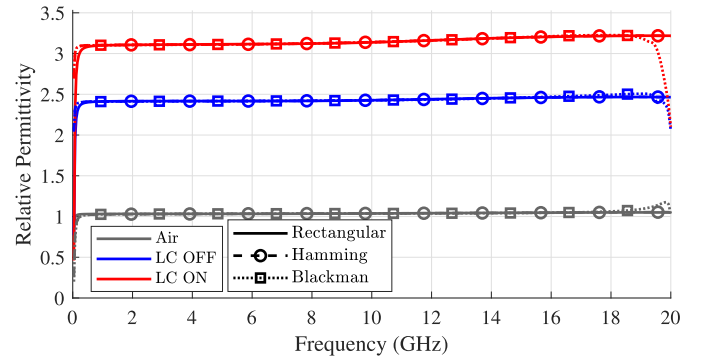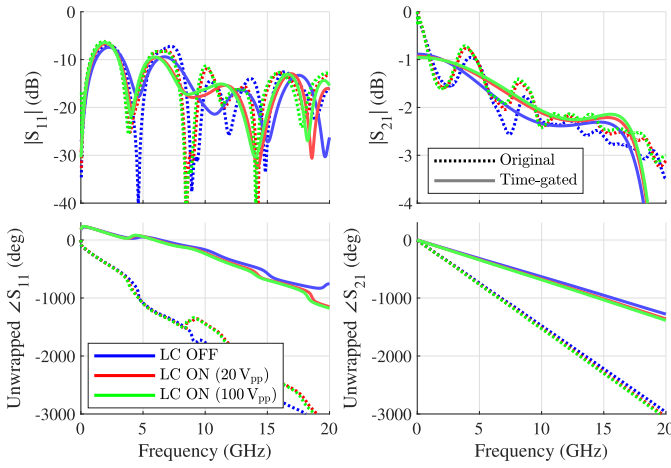
Fig. 7. Original and time-gated measured S-parameters for the ON and OFF LC states.
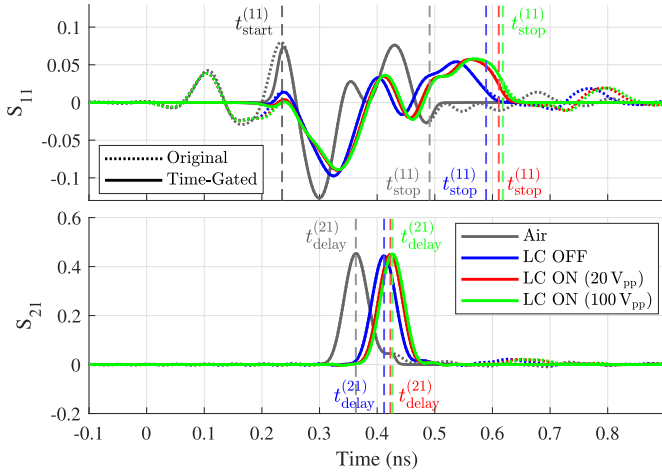

Fig. 8. Widened impulse responses of the measured S_{11} (up) and S_{21} (down) before and after the time gating, and with their timestamps.
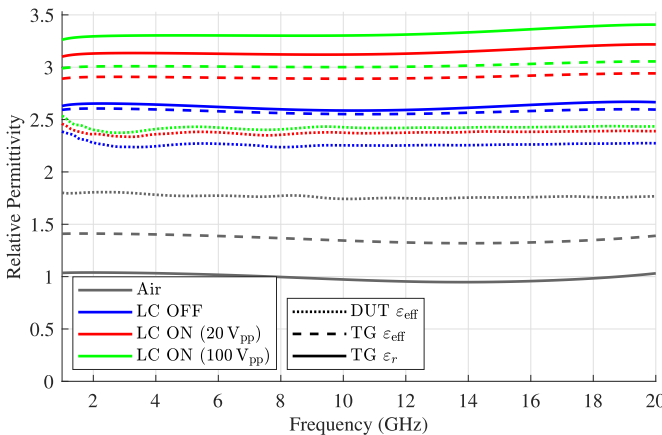

Fig. 9. Effective and relative permittivities obtained from the original and time-gated measurements for different pool substrate scenarios.

Fig. 10. Temporal change in the calculated permittivity of the LC from OFF- to ON-states and vice versa for 20-V_{pp} (top) and 100-V_{pp} (bottom) bias voltages.

obtained for the 100-V_{pp} bias signal indicate that the 20-V_{pp} bias was insufficient to polarize the LC fully. Furthermore, the achieved permittivity value is very similar to the simulation one (taking into account fabrication tolerances) and, so, less than $\varepsilon_{r_\parallel}$, due to the inhomogeneous LC polarization by the narrow microstrip. These results show the achievable ε_r values for this physical configuration.

The results could be different if another type of geometry (for example, other transmission lines, substrate height, or microstrip width) was used, a problem arising from the anisotropic physical properties of the LCs. However, the aim of this work has been focused on extracting the achievable permittivities for any specific structure considered as a transmission line, which can significantly facilitate the work of researchers to know the effective range of variation of the relative permittivity of crystals when designing reconfigurable devices. For instance, if a leaky-wave antenna based on a periodically loaded microstrip line is built, this experiment is of direct utility to have a model for the LC permittivity and be able to design the reconfigurability range of its beam directions.

Using a script to periodically save measurements while the LC is being polarized and processing each of them, the LC permittivity's time evolution is obtained, as shown in Fig. 10 for both polarization voltages. A higher bias voltage achieves not only a greater permittivity but also a faster polarization response (10%–90% response time of 68 s for 20 V_{pp} and less than 3 s for 100 V_{pp}), as is the expected behavior for this GT7-29001 LC presenting elastic constants $K_{11} = 14.3$ pN and $K_{33} = 18.7$ pN, rotational viscosity $\gamma = 316$ mPa s, and threshold voltage $V_{th} = 0.85$ V. The return to the OFF-state has a similar evolution in both cases, with a response time around 350 s. These values are in close agreement with the theoretical expressions from [1].

V. CONCLUSION

In this work, an efficient method for characterizing the dielectric permittivity of nematic LCs in broadband has been

considerably similar to those from simulations in Fig. 5. The fact that the OFF-state presents an $\varepsilon_{r_\parallel} > \varepsilon_{r_{OFF}} > \varepsilon_{r_\perp}$ is mainly due to the high pool thickness, which prevents the rubbed Kapton layer from correctly orienting the LC molecules that are far from it, thus realizing an intermediate permittivity given by a $\theta_m > 0°$. For the ON-state, the higher values
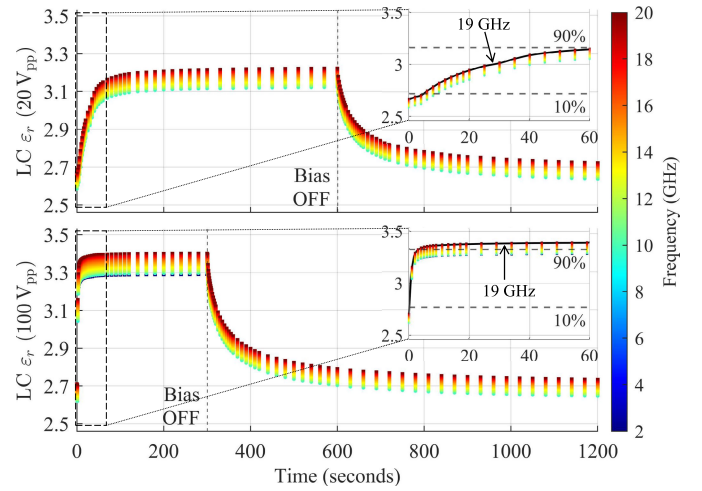
introduced, contributing to the advancement of reconfigurable devices for microwave and millimeter-wave applications. The approach uses additive manufacturing technology to fabricate a microstrip line that accommodates LCs, making it easy to polarize and achieve a dynamic modulation of its permittivity. Using additive manufacturing and eliminating thru–reflect–line (TRL) calibration in favor of time gating offer a practical and effective approach for efficiently characterizing LC-based reconfigurable devices. The validity of this method has been assessed through a comprehensive evaluation involving a combination of simulations and experimental measurements. The results are reliable, demonstrating the accuracy of the proposed technique, which is more straightforward than others found in the state of the art.

Acknowledgment

References

[1] D. C. Zografopoulos, A. Ferraro, and R. Beccherelli, "Liquid-crystal high-frequency microwave technology: Materials and characterization," *Adv. Mater. Technol.*, vol. 4, no. 2, Feb. 2019, Art. no. 1800447.

[2] A. Alex-Amor, Á. Palomares-Caballero, A. Palomares, A. Tamayo-Domínguez, J. M. Fernández-González, and P. Padilla, "Generalized director approach for liquid-crystal-based reconfigurable RF devices," *IEEE Microw. Wireless Compon. Lett.*, vol. 29, no. 10, pp. 634–637, Oct. 2019.

[3] G. Perez-Palomino et al., "Accurate and efficient modeling to calculate the voltage dependence of liquid crystal-based reflectarray cells," *IEEE Trans. Antennas Propag.*, vol. 62, no. 5, pp. 2659–2668, May 2014.

[4] R. Guirado, P. De la Rosa, G. Perez-Palomino, M. Caño-García, E. Carrasco, and X. Quintana, "Characterization and application of dual frequency liquid crystal mixtures in mm-wave reflectarray cells to improve their temporal response," *IEEE Trans. Antennas Propag.*, vol. 71, no. 8, pp. 6535–6545, Aug. 2023.

[5] R. Tchema, N. C. Papanicolaou, and A. C. Polycarpou, "An investigation of the dynamic beam-steering capability of a liquid-crystal-enabled leaky-wave antenna designed for 5G applications," *Appl. Phys. Lett.*, vol. 119, no. 3, Jul. 2021, Art. no. 034104.

[6] E. Abdo-Sanchez, A. Epstein, and G. V. Eleftheriades, "Reconfigurability mechanisms with scanning rate control for omega-bianisotropic huygens' metasurface leaky-wave antennas," *IEEE Access*, vol. 7, pp. 168247–168260, 2019.

[7] F. Kamrath et al., "Bandwidth and center frequency reconfigurable waveguide filter based on liquid crystal technology," *IEEE J. Microw.*, vol. 2, no. 1, pp. 134–144, Jan. 2022.

[8] Q. Wang, Z. Su, S. Li, Y. Su, H. Zhao, and X. Yin, "Electrically tunable phase shifter with improved phase-shifting capability based on liquid crystal," *IEEE Microw. Wireless Technol. Lett.*, vol. 33, no. 5, pp. 527–530, May 2023.

[9] J. Parka, J. Krupka, R. Dąbrowski, and J. Wosik, "Measurements of anisotropic complex permittivity of liquid crystals at microwave frequencies," *J. Eur. Ceram. Soc.*, vol. 27, nos. 8–9, pp. 2903–2905, Jan. 2007.

[10] A. Alex-Amor, A. Palomares-Caballero, F. Mesa, O. Quevedo-Teruel, and P. Padilla, "Dispersion analysis of periodic structures in anisotropic media: Application to liquid crystals," *IEEE Trans. Antennas Propag.*, vol. 70, no. 4, pp. 2811–2821, Apr. 2022.

[11] H. Peng, Y. Zhang, S. Zhu, M. Temiz, and A. El-Makadema, "Determining dielectric properties of nematic liquid crystals at microwave frequencies using inverted microstrip lines," *Liquid Crystals*, vol. 49, no. 15, pp. 2069–2081, Dec. 2022.

[12] M. Yazdanpanahi, S. Bulja, D. Mirshekar-Syahkal, R. James, S. E. Day, and F. A. Fernandez, "Measurement of dielectric constants of nematic liquid crystals at mm-wave frequencies using patch resonator," *IEEE Trans. Instrum. Meas.*, vol. 59, no. 12, pp. 3079–3085, Dec. 2010.

[13] V. Nova, C. Bachiller, B. Villacampa, R. Kronberger, and V. E. Boria, "Characterization of nematic liquid crystals at microwave frequencies," *Crystals*, vol. 10, no. 12, p. 1106, Dec. 2020.

[14] P. Deo, D. Mirshekar-Syahkal, L. Seddon, S. E. Day, and F. A. Fernández, "Microstrip device for broadband (15–65 GHz) measurement of dielectric properties of nematic liquid crystals," *IEEE Trans. Microw. Theory Techn.*, vol. 63, no. 4, pp. 1388–1398, Apr. 2015.

[15] M. El Kadiri, J. P. Parneix, and A. Chapoton, "General time domain analysis of T.D.S. data: Application to liquid crystals," *IEEE Trans. Instrum. Meas.*, vol. IM-34, no. 1, pp. 70–74, Mar. 1985.

[16] K. M. Fidanboylu, S. M. Riad, and A. Elshabini-Riad, "An enhanced time-domain approach for dielectric characterization using stripline geometry," *IEEE Trans. Instrum. Meas.*, vol. 41, no. 1, pp. 132–136, Mar. 1992.

[17] B. Archambeault, S. Connor, and J. C. Diepenbrock, "Time domain gating of frequency domain S-parameter data to remove connector end effects for PCB and cable applications," in *Proc. IEEE Int. Symp. Electromagn. Compat.*, Feb. 2006, pp. 199–202.

[18] A. M. H. Nasr, A. Y. Nashashibi, and K. Sarabandi, "Ultrawideband characterization of complex dielectric constant of planar materials for 5G applications," *IEEE Trans. Instrum. Meas.*, vol. 70, pp. 1–11, 2021.

[19] H.-J. Eul and B. Schiek, "A generalized theory and new calibration procedures for network analyzer self-calibration," *IEEE Trans. Microw. Theory Techn.*, vol. 39, no. 4, pp. 724–731, Apr. 1991.

[20] K. J. Silvonen, "Calibration of test fixtures using at least two standards (microwave circuits)," *IEEE Trans. Microw. Theory Techn.*, vol. 39, no. 4, pp. 624–630, Apr. 1991.

[21] M. Pérez-Escribano and E. Márquez-Segura, "Random errors in broadband characterization of the propagation constant of transmission lines using multiple two-port measurements," *IEEE Access*, vol. 9, pp. 59038–59047, 2021.

[22] M. Pérez-Escribano and E. Márquez-Segura, "End-launcher repeatability in broadband methods for characterization of the propagation constant of transmission lines using two-port measurements," *IEEE Trans. Instrum. Meas.*, vol. 71, pp. 1–4, 2022.

[23] M. Pérez-Escribano and E. Márquez-Segura, "Parameters characterization of dielectric materials samples in microwave and millimeter-wave bands," *IEEE Trans. Microw. Theory Techn.*, vol. 69, no. 3, pp. 1723–1732, Mar. 2021.

[24] Cadence®. *TDR Gating Python Script—AWR Scripts*. Accessed: Oct. 27, 2023. [Online]. Available: https://kb.awr.com/display/awrscripts/TDR

[25] M. A. Couker and L. J. Kushner, "A microstrip phase-trim device using a dielectric overlay," *IEEE Trans. Microw. Theory Techn.*, vol. 42, no. 11, pp. 2023–2026, Nov. 1994.

[26] A. K. Verma and G. H. Sadr, "Unified dispersion model for multilayer microstrip line," *IEEE Trans. Microw. Theory Techn.*, vol. 40, no. 7, pp. 1587–1591, Jul. 1992.

[27] D.-K. Yang and S.-T. Wu, *Fundamentals of Liquid Crystal Devices* (Wiley SID series in display technology). Hoboken, NJ, USA: Wiley, 2006.

[28] R. Guirado et al., "Dynamic modeling of liquid crystal-based metasurfaces and its application to reducing reconfigurability times," *IEEE Trans. Antennas Propag.*, vol. 70, no. 12, pp. 11847–11857, Dec. 2022.

Pablo Mateos-Ruiz was born in Melilla, Spain, in 1997. He received the B.S. and M.Sc. degrees in telecommunication engineering from Universidad de Málaga, Málaga, Spain, in 2019 and 2021, respectively. He is currently pursuing the Ph.D. degree in telecommunication engineering from the University of Málaga, Malaga.

Since 2018, he has been a Research Assistant with the Departamento de Ingeniería de Comunicaciones, Universidad de Málaga, with different scholarships. In 2021, he carried out his master's thesis as a granted student at German Aerospace Center (DLR), Institute of Navigation and Communication, Munich, Germany. His research interests focus on circuit modeling, and planar and metasurface-based antennas.

Mr. Mateos-Ruiz has been receiving the Formación de Profesorado Universitario (FPU) Scholarship from Spanish Ministerio de Ciencia, Innovación y Universidades, since 2021.

Mario Pérez-Escribano was born in Alcalá la Real, Jaén, Spain, in 1993. He received the B.S. degree in telecommunication engineering from the University of Málaga, Málaga, Spain, in 2015, the M.S. degree in telecommunication engineering from University Carlos III de Madrid, Madrid, Spain, in 2017, and the Ph.D. degree from the Departamento de Ingeniería de Comunicaciones, Escuela Técnica Superior de Ingeniería (ETSI) de Telecomunicación, Universidad de Málaga, in 2022.

In 2023, he joined the SWT Group, Department of Signal Theory, Telematics and Communications, University of Granada, Granada, Spain, where he is currently doing a postdoctoral research stay. His research interests are focused on equivalent circuits and time-modulated structures.

Dr. Pérez-Escribano was a recipient of Spanish Ministry of Education, Culture, and Sports Scholarship for the term 2017–2022 and the Margarita Salas Fellowship from 2023 to 2024.

Alberto Hernández-Escobar received the B.E., M.Sc., and Ph.D. degrees in telecommunication engineering from the Universidad de Málaga, Málaga, Spain, in 2014, 2016, and 2021, respectively.

In 2014, he joined the Department of Communications Engineering, Universidad de Málaga, as a Research Assistant. In 2016, he was a granted student at the Department of Electronic Systems, Aalborg University, Aalborg, Denmark. From September to December 2018, he was a Visiting Ph.D. Student at the Department of Electrical Engineering, KU Leuven, Leuven, Belgium. He has been a Post-Doctoral Fellow at Tokyo Institute of Technology, Tokyo, Japan, since 2022. His research interests focus on the analysis, circuit modeling, design, and application of planar antennas.

Dr. Hernández-Escobar was a recipient of the Ministerio de Educación, Cultura y Deporte Scholarship (2016–2021). He has been receiving the Horizon Europe Marie Skłodowska-Curie Fellowship since 2023.

Elena Abdo-Sánchez (Member, IEEE) received the M.Sc. and Ph.D. degrees in telecommunication engineering from the Universidad de Málaga, Málaga, Spain, in 2010 and 2015, respectively.

In 2009, she was a granted student with German Aerospace Center (DLR), Institute of Communications and Navigation, Munich, Germany. In 2010, she joined the Department of Communication Engineering, Universidad de Málaga, where she became an Associate Professor, in 2021. From April 2013 to July 2013, she was a Visiting Ph.D. Student with the Antennas and Applied Electromagnetics Laboratory, University of Birmingham, Birmingham, U.K. From May 2016 to May 2017, she was a Marie Skłodowska-Curie Post-Doctoral Fellow with the Electromagnetics Group, University of Toronto, Toronto, ON, Canada. Her research interests focus on the electromagnetic analysis and design of planar antennas and the application of metasurfaces to the implementation of novel antennas.

Dr. Abdo-Sánchez was a recipient of the Junta de Andalucía Scholarship from 2012 to 2015, the Marie Skłodowska-Curie Fellowship from 2016 to 2018, and the Juan de la Cierva Fellowship from 2020 to 2021.

Enrique Márquez-Segura (Senior Member, IEEE) was born in Málaga, Spain, in 1970. He received the Ingeniero de Telecomunicación and Doctor Ingeniero degrees from the Universidad de Málaga, Málaga, in 1993 and 1998, respectively.

In 1994, he joined the Departamento de Ingeniería de Comunicaciones, Escuela Técnica Superior de Ingeniería (ETSI) de Telecomunicación, Universidad de Málaga, where he became an Associate Professor, in 2001. His current research interests include electromagnetic material characterization; additive manufacturing; measurement techniques; and RF, microwave, and millimeter-wave circuits design for communication applications.

Dr. Márquez-Segura was a recipient of Spanish Ministry of Education and Science Scholarship for the term 1994–1995.

Teresa M. Martín-Guerrero (Senior Member, IEEE) was born in Málaga, Spain. She received the Grado de Licenciado en Ciencias Físicas (M.Sc. equivalent in physics) from the Universidad de Granada, Granada, Spain, in 1990, and the Grado de Doctor Ingeniero de Telecomunicación (Ph.D. equivalent in telecommunication engineering) from the Universidad de Málaga, Málaga, in 1995.

In 1991, she joined the Departamento de Ingeniería de Comunicaciones, Universidad de Málaga, where she became a Full Professor, in 2016. Since February 2023, she has been the Head of the Departamento de Ingeniería de Comunicaciones, Universidad de Málaga. She has been the Chair of the 13th European Microwave Integrated Circuits Conference (EuMIC), Madrid, in September 2018. Her current research interests include microwave and millimeter-wave device characterization; and modeling, analysis, and design of RF nonlinear circuits.

Carlos Camacho-Peñalosa (Life Senior Member, IEEE) received the Ingeniero de Telecomunicación and Dr.-Ing. degrees from the Universidad Politécnica de Madrid, Madrid, Spain, in 1976 and 1982, respectively.

From 1976 to 1989, he was with the Escuela Técnica Superior de Ingenieros de Telecomunicación, Universidad Politécnica de Madrid, as a Research Assistant, an Assistant Professor, and an Associate Professor. From September 1984 to July 1985, he was a Visiting Researcher with the Department of Electronics, Chelsea College, University of London, London, U.K. In 1989, he became a Full Professor with the Universidad de Málaga, Málaga, Spain. He was the Director of the Escuela Técnica Superior de Ingeniería de Telecomunicación from 1991 to 1993, the Vice-Rector from 1993 to 1994, and the Deputy Rector of the Universidad de Málaga in 1994. From 1996 to 2004, he was the Director of the Departamento de Ingeniería de Comunicaciones, Universidad de Málaga. From 2000 to 2003, he was the Co-Head of the Nokia Mobile Communications Competence Center, Málaga. His research interests include microwave and millimeter solid-state circuits, nonlinear systems, and applied electromagnetism. He has been responsible for several research projects on nonlinear microwave circuit analysis, microwave semiconductor device modeling, and applied electromagnetics.